*J Mater Sci: Mater Electron* (2020) 31:21035–21045

# Electro-codeposition of $V_2O_5$-polyaniline composite on Ni foam as an electrode for supercapacitor

Asma Aamir[1,2], Adil Ahmad[2], Said Karim Shah[3], Noor ul Ain[1], Mazhar Mehmood[4], Yaqoob Khan[2,*], and Zia ur Rehman[1,*]

[1] *Department of Chemistry, Quaid-i-Azam University, Islamabad 45320, Pakistan*
[2] *Nanosciences and Technology Department, National Center for Physics, QAU Campus, Islamabad 45320, Pakistan*
[3] *Department of Physics, Faculty of Physical and Numerical Sciences, Abdul Wali Khan University, Mardan, KPK 23200, Pakistan*
[4] *Department of Metallurgy and Materials Engineering, National Centre for Nanotechnology, Pakistan Institute of Engineering and Applied Sciences, P. O Nilore, Islamabad 45650, Pakistan*

**Received:** 19 April 2020
**Accepted:** 5 October 2020
**Published online:** 23 October 2020



## ABSTRACT

To fulfill the increasing energy demand, it is necessary to develop such an electrode material for pseudocapacitors having a high energy density, better cycle life, and potential for commercialization. Herein, we report an electro-codeposition technique to fabricate a high-performance $V_2O_5$-PANi composite deposited on the metallic Nickel foam substrate as an electrode for pseudocapacitors. Ni foam serves as a porous and conductive framework and therefore shortens the ions diffusion pathway. Composite shows good performance than pure $V_2O_5$ and PANi due to their synergistic effect. X-ray diffraction (XRD) and energy dispersive X-ray spectroscopy (EDX) analysis have confirmed the successful incorporation of metal oxide into the polymer backbone. Moreover, $V_2O_5$-PANi composite exhibited a very wide voltage window of 2.5V (between − 1 and 1.5V vs. SCE), the highest specific capacitance of 1115 F/g, and less charge transfer resistance. The ability to prepare composite electrodes with high performance *via* a binder-free electro-codeposition technique could open up new prospects for high energy density pseudocapacitors.

## 1 Introduction

The demand for high-performance energy storage devices such as supercapacitor and batteries increases with prompt progress in the hybrid electric vehicles (HEV) and portable electronic devices [1–4]. A supercapacitors (SCs) have potential usage in backup power source, electronic fuses, and power supply devices for electric vehicles due to their long cycle life, fast charge/discharge rates, high power density, and low cost of maintenance [5–7]. However, batteries have high energy density than supercapacitors [8, 9]. On the basis of electrode material and energy storage mechanism, SCs are divided into two types: electric double-layer capacitor (EDLC) and pseudocapacitors (PCs) [10, 11]. EDLCs employ

Address correspondence to E-mail: yaqoob@ncp.edu.pk; zrehman@qau.edu.pk; hafizqau@yahoo.com

https://doi.org/10.1007/s10854-020-04616-9

carbon-based material as an electrode due to their large surface area for energy storage ensured by the accumulation of ions to form an electrical double-layer at the interface of electrolyte and electrode. Examples of electrode materials include carbon nanotubes, activated carbon, graphene, carbon ion. For such electrode materials, power density and cycling stability of EDLCs are high [12, 13], but their energy density and specific capacitance are lower than PCs due to the accumulation of charges restricted only to the surface [14], leaving the bulk of materials unused. However, the high cost and the complication of production procedures for carbon-based materials significantly affects their practical use in supercapacitors for industrial applications. Therefore, it is necessary to search exponential active electrode materials to improve the performance of current collecting electrode that can significantly affect real-time applications of SCs [15]. It is also well known that electrode materials play a crucial role in the electrochemical performance of the energy storage devices [16]. PCs are based on redox-active transition metal oxides [17, 18] and conducting polymers materials for energy storage *via* faradaic reactions [19–21]. Ruthenium oxide was the first metal oxide to be used as an electrode for PCs giving specific capacitance of 600–1000 F/g in the voltage window of 1.4 V [22], but its commercial utilization has been restricted owing to its high cost. Other low-cost transition metal oxides such as $MnO_x$, $CrO_x$, $CoO_x$, NiO, $NiCoO_2$, and $V_2O_5$, have also been studied as electrode materials for PCs [23–27]. Recently, layered double metal hydroxides (CoMn-LDH@$MnO_2$) and mixed metal oxide and sulfides have also been investigated as electrode materials for supercapacitors [28, 29]. Among transition metals, Vanadium oxide has gained much attention owing to its layered structure, undergoing easy diffusion of lithium ions in and out of the structure, and attainment of high capacitance due to its multiple oxidation states. The high oxidation state of vanadium leads to the probability of multiple electrons storage per formula unit. However, the electronic conductivity of vanadium oxide is low. It has been described that electro-spun $V_2O_5$ nanofibers displayed excellent stability in the voltage window between − 1 and 0 V vs. SCE [30]. Moreover, $V_2O_5$-polypyrrole nanocomposite exhibited a specific capacitance of 308 F/g in a wide voltage range, from − 0.9 to 0.1 V vs. SCE [31].

Moreover, different conducting or conjugated polymers such as polypyrrole (Ppy), polyaniline (PANi), and their derivatives have been investigated for PCs due to their high specific capacitance [32–34]. Electroconducting polymer such as PANi is well-known among recently developed electrode material for pseudocapacitor. It has the advantages of highly reversible charge storage ability, high thermal stability, notable applications in energy storage technology [35, 36], ease of synthesis and high capacitance (3407 F/g) [37]. The PANi is affordable as it composed of cheap components including C, H, N or S. However, long-term degradation and shrinkage upon cycling are the associated drawbacks with these conducting polymers [38].

Recently, composite materials based on transition metal oxides and conducting polymers have gained significant consideration, as they can combine the benefits of both constituents providing superior properties. Composite has a synergistic effect over enhancing the surface area, minimizing particle size, preventing particle agglomeration, improving cyclic stability and providing extra pseudo capacitance. In composite form conceivable role of both components is; metal oxide provides structural and mechanical support to conducting polymer and acts as a charge storage material whereas conducting polymer offers good electrical conductivity owing to its flexible and polymeric nature. Hence, significantly improved performance is expected in composite form than the individual component material. Composites of PANi and carbon-based material have been synthesized via in situ chemical oxidation of co-polymerization method, however, the same method has rarely been employed for the combination of metal oxides and PANi [39]. This may be due to the reason that the formation of metal oxides generally requires a mild alkaline environment while the polymerization of PANi proceeds under an acidic condition. Fortunately, one step electro deposition method can still be carried out for combining certain transition metal oxides with PANi, as long as the voltage ranges for the deposition of both the components coincide [40] and the subsequent composite remains insoluble in the electrolytes. Moreover, the synthesis of nanostructural materials with pores or voids (porous materials) can enhance interactions of electrode/electrolyte interface, delivering low internal resistance and rapid ionic diffusion paths for better electrochemical performances including maximum

specific capacitance and good energy and power density [41].

In the present work, a binder-free electro-codeposition of $V_2O_5$-PANi composite on nickel foam as a conducting substrate has been carried out for the fabrication of electrode material. In the conventional route, a binder is added to an active material for proper adhesion between different constituents which negatively affect the electrochemical performance of electrode, as they do not add to charge storage, but increase the interfacial stress and ohmic résistance causing the failure of PCs. Moreover, the electrochemical polymerization of PANi is a quicker and environmentally benevolent polymerization route, devoid of additives and oxidants.

## 2 Experimental

### 2.1 Electro-codeposition

Cyclic voltammetry of $V_2O_5$-PANi composite was carried out using Gamry Ref-3000 Potentiostat/Galvanostat in a three-electrode set up with Ni foam as working electrode, Saturated Calomel Electrode (SCE) as a reference electrode and graphite rod as a counter electrode. Prior to electro-codeposition, Ni foam was ultrasonicated in 0.1 M $H_2SO_4$ solution, washed with deionized (DI) water, ultrasonicated in acetone and methanol for 30 min, again washed with DI water, and dried in $N_2$ flow at 100 °C for 30 min. An aqueous solution of 0.1 M Vanadyl sulfate and 0.05 M Aniline was used as an electrolyte for the electro-codeposition of PANi-Vanadium oxide in the potential range of − 2 to 1.6 V. Electrodeposited samples were rinsed with DI water followed by annealing at 300 °C for 3 h in a tube furnace. The quantity of $V_2O_5$-PANi composite deposited was evaluated by measuring the difference between the weight of bare foam and $V_2O_5$ deposited foam after annealing. The annealed sample was further used for structural, morphological, and electrochemical testing.

### 2.2 Characterization

The phase and crystal structure, elemental composition, and morphological studies were done using X-ray diffraction (XRD), Energy Dispersive Spectroscopy (EDX), and Field Emission Scanning Electron Microscopy (FESEM).

### 2.3 Electrochemical testing

The electrochemical performance was investigated in a conventional three-electrode cell with $V_2O_5$-PANi composite deposited Ni foam as working electrode, graphite rod as a counter, saturated calomel electrode (SCE) as the reference electrode and 0.5 M $LiClO_4$ dissolved in Propylene carbonate as an electrolyte. Cyclic voltammetry (CV), Galvanostatic charge-discharge (GCD), and Electrochemical impedance spectroscopy (EIS) measurement were carried out to explore the charge-discharge capability, reversibility, and other electrochemical properties. Gamry Ref-3000 Potentiostat/Galvanostat was operated for all electrochemical characterization. The gravimetric discharge capacitance was calculated from GCD according to the following formula:

$$Csp = \frac{I \times t}{m \times V} \quad (1)$$

where $C_{sp}$, $I$, $t$, $m$ and $V$ symbolize the specific capacitance ($F/g$), current density ($A/g$), discharge time (seconds), mass of the active material loaded (gram) and discharge potential windows (volts), respectively.

## 3 Results and discussion

Figure 1 shows the cyclic voltammetric deposition of the composite. In the initial cycle, high oxidation current was observed owing to the higher conductivity of Ni foam as deposition process of the aniline and $VO^{2+}$, responsible for diminution of conductivity, was just initiated. However, the efficiency and hence the oxidation currents decreased in the proceeding cycles due to a decrease in the conductivity of foam by the deposited $V_2O_5$-PANi composite. The amount of deposited material increases with the successive number of cycles, thus degrading substrate conductance. As a result, the currents decreased and saturated in the 25th cycle. Moreover, the electrode resistance increases which by deposition up-shifted the oxidation potential.

XRD analysis was carried out to investigate the structure of $V_2O_5$-PANi composite. Figure 2 shows the typical XRD pattern of $V_2O_5$-PANi annealed at

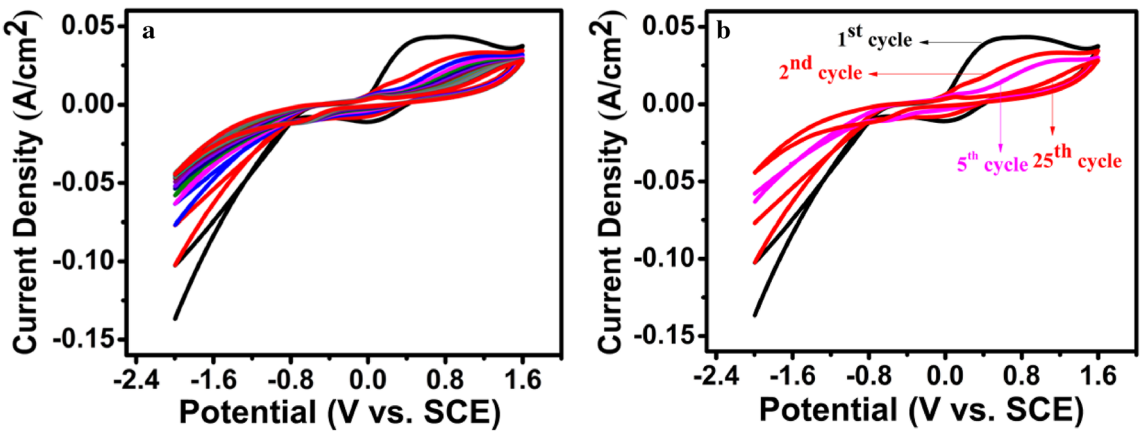


**Fig. 1** **a** Cyclic voltammetric deposition of $V_2O_5$-PANi composite at a scan rate of 50 mV/s, **b** showing number of cycles

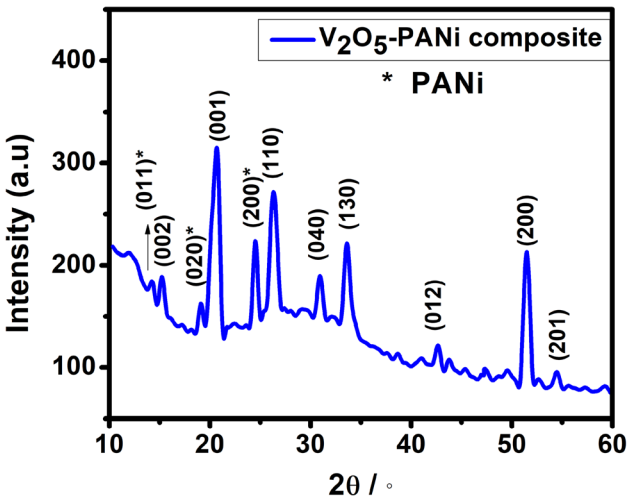


**Fig. 2** XRD pattern of electrodeposited $V_2O_5$-PANi composite electrode

300 °C for 3 h with diffraction peaks between 14° to 30° corresponding to perpendicular and parallel periodicity of the polyaniline chain [34]. Peaks at 14°, 19° and 25° marked as asterisk for PANi corresponds to (011), (020), and (200) crystal planes [42–44]. The peak at 15.6°, 20.4°, 21.9°, 26.3°, 31.2°, 34.3°, 52.3°, and 54.8° corresponds to (002), (001), (110), (040), (130), (012), (200), and (201) plan for orthorhombic $V_2O_5$ crystal structure (JCPDS no 41-1426) [45].

Morphology and size of the particles affect the electrochemical performance of the electroactive material significantly and the formation of small size particles can enhance such behavior. The morphology of $V_2O_5$/PANi composite has been investigated using FESEM technique. Figure 3 presents the morphology of the deposits with an average particle size of ~ 200 nm. The particles possess spherical plate shape morphology with voids that permit easy

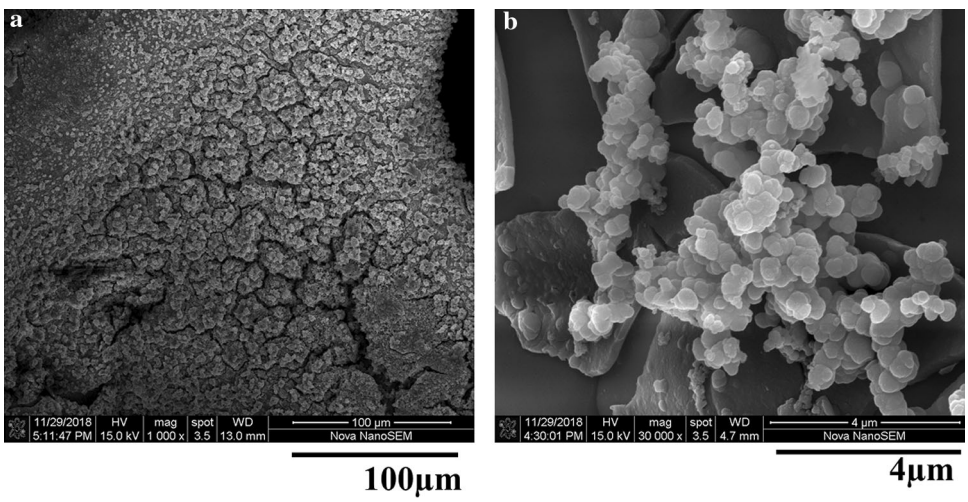


**Fig. 3** FESEM images of electrodeposited $V_2O_5$-PANi composite, **a** part of Nickel foam showing thick deposition and **b** showing plates morphology of composite

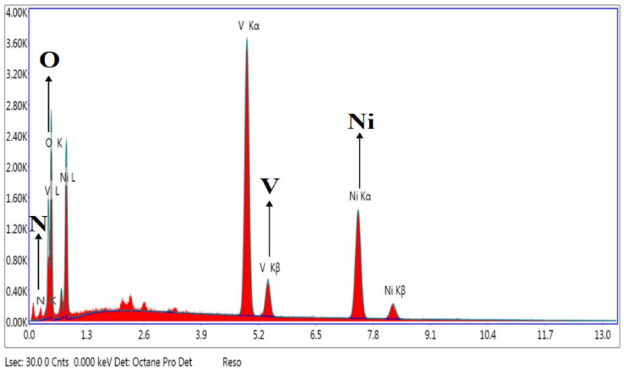


**Fig. 4** EDX spectra of $V_2O_5$-PANi composite deposited on Ni foam

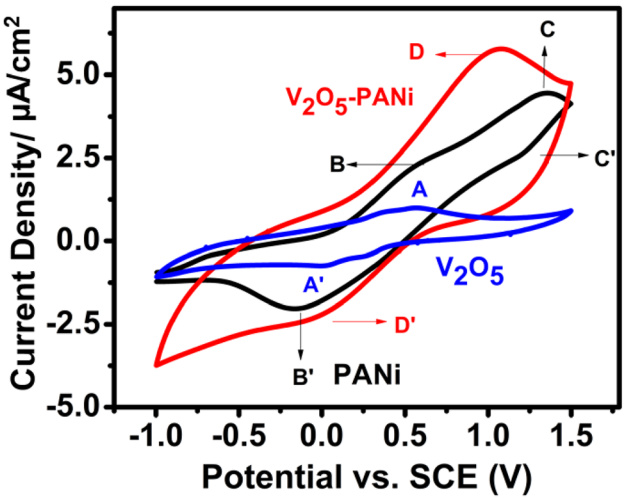


**Fig. 5** Cyclic Voltammogram of $V_2O_5$, PANi and $V_2O_5$-PANi composite

transport of ions of electrolytes for charge storage and also make use of the bulk of the material.

Figure 3a shows part of Nickel foam with a layer of thick deposition for maximum number of charge-discharge cycles to be carried out resulting in longer cycle life of the electrode. Moreover, this type of nanostructure does not impede the transport of $Li^+$ ions and electrons between the PANi surface and electrolyte, sustaining the faradaic pseudocapacitive property of $V_2O_5$ and PANi.

Figure 4 displays the EDX spectrum confirming the presence of Vanadium, Oxygen, Nickel, and Nitrogen (from PANi), which assures the successful electro-codepositions of $V_2O_5$ on Nickel foam.

To investigate the electrochemical behavior of $V_2O_5$-PANi composite, cyclic voltammetry (CV) was performed in 0.5 M $LiClO_4$ in propylene carbonate solution in a potential range of − 1.5 to 1.5 V. The exposed area for the electrolyte of the working electrode was 1 $cm^2$. The CV of $V_2O_5$, PANi, and $V_2O_5$-PANi composite is shown in Fig. 5. The CV shows a pair of redox peaks A and A′ corresponding to Li removal and insertion in the layered $V_2O_5$ material [46, 47]. The peaks B/B′ correspond to switching between leucoemeraldine and emeraldine form while peaks C/C′ correspond to transition between emeraldine and pernigraniline form of PANi [5, 40, 48]. Cyclic voltammogram of $V_2O_5$-PANi composite displays a combined shape of $V_2O_5$ and PANi verifying the successful incorporation of $V_2O_5$ into polyaniline. CV curves demonstrate that only $V_2O_5$ and PANi contribute towards capacitance. There is no contribution from Ni foam as no peak around 0.3 V corresponding to the conversion of NiO to NiOOH

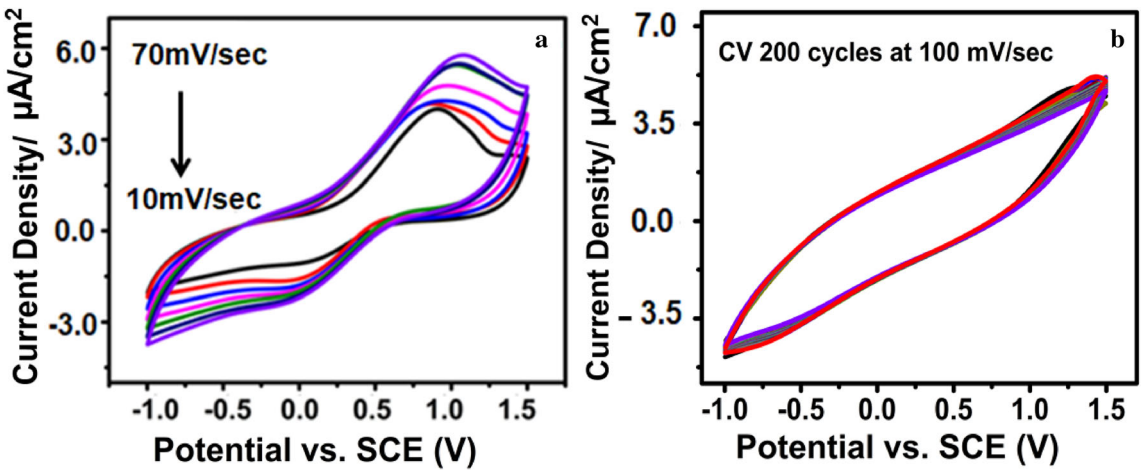


**Fig. 6** **a** Cyclic voltammogram at different scan rates and **b** CV 200 cycle of $V_2O_5$-PANi composite

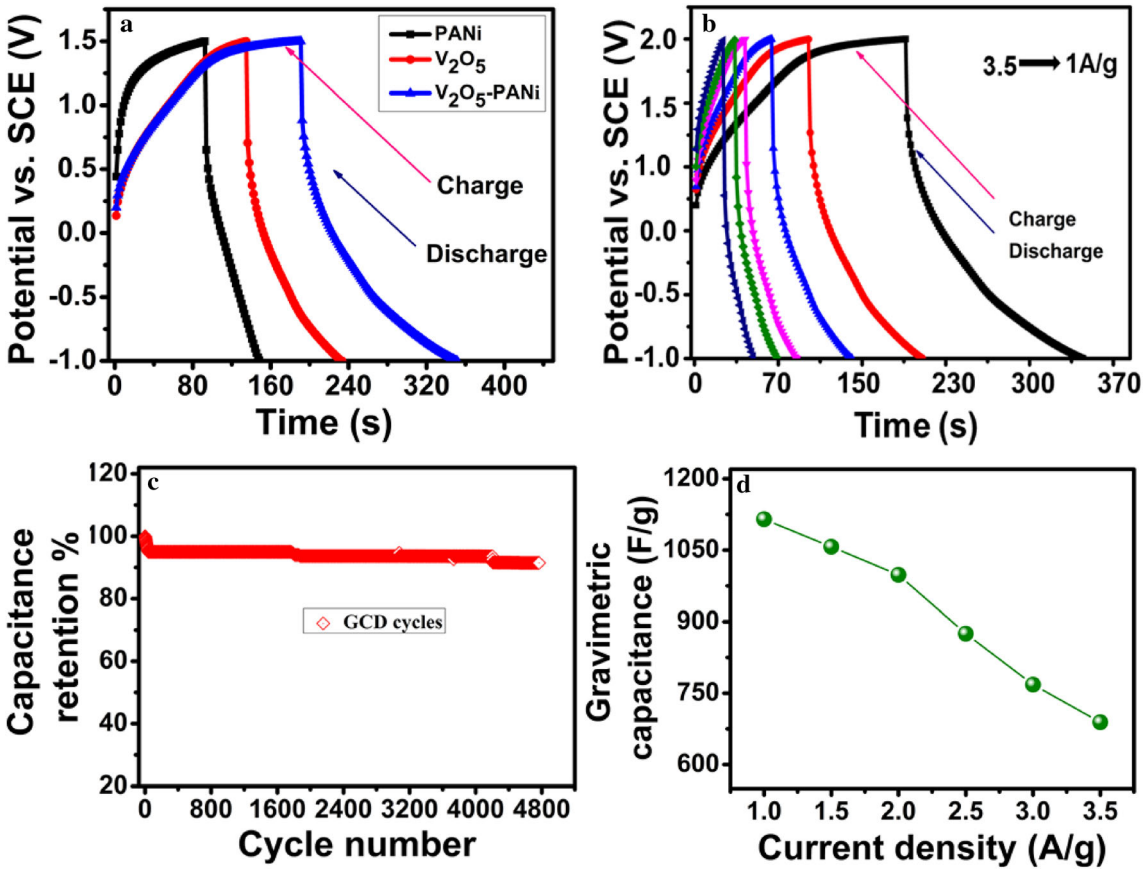


**Fig. 7** **a** GCD curve of $V_2O_5$, PANi and $V_2O_5$-PANi composite at a current density of 1 mA/cm$^2$, **b** GCD of $V_2O_5$-PANi composite at different current densities, **c** retention of capacitance of 5000 GCD cycles vs. cycle number of composite and **d** Variation of gravimetric capacitance with current density

**Table 1** Comparison of similar reported $V_2O_5$-PANi composite for supercapacitors

| S. No. | $V_2O_5$-PANi composite | Current Density (A/g) | Specific capacitance (F/g) | Ref. |
|---|---|---|---|---|
| 1 | $V_2O_5$-PANi composite nanowires | 1 | 538 | [40] |
| 2 | $V_2O_5$-PANi composite micro-fibrillar | 1 | 450 | [57] |
| 3 | $V_2O_5$-PANi composite nanoplates | 1 | 1115 | Present work |

redox process was observed [49]. The CV profiles of all three samples are noticeably different from that of pure electric double-layer capacitors which are generally ideal rectangles. This suggests the progression of redox reaction in the electrodes and the pseudo-capacitive nature of electroactive material [50]. From the CV profile, it can be clearly seen that the composite possess a higher capacitive current and larger CV integration area required for desirable capacitance. Notably, the composite electrode possesses better electrochemical activity owing to the synergistic effect of PANi and $V_2O_5$ with the largest voltage window of 2.5 V. The widening of working voltage is possibly induced by the combination of high oxygen over potential and hydrogen evolution voltage offered by PANi and $V_2O_5$ under positive and negative polarization, respectively.

Figure 6a shows the CV of $V_2O_5$-PANi composite at different scan rates from 10 to 70 mV/sec. CV profile at different scan rates has the same shape within the potential range of − 1 to 1.5 V vs. SCE in a $LiClO_4$ in propylene carbonate electrolyte revealing

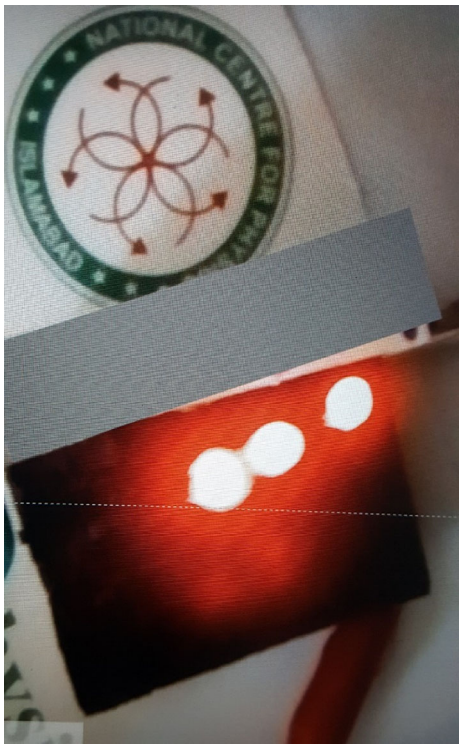

**Fig. 8** Illumination of 3 LEDs using 2 electrode device of $V_2O_5$-PANi nanocomposite and graphite

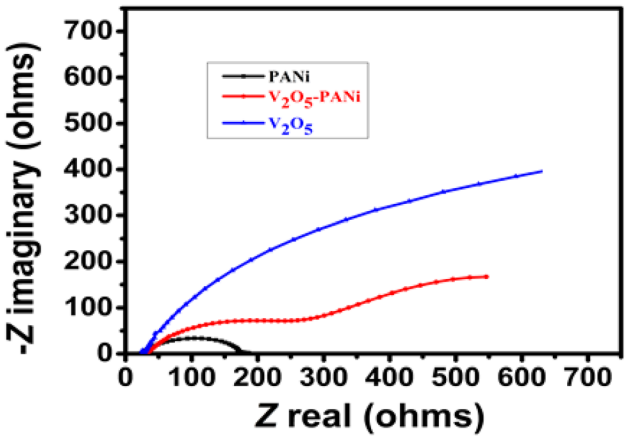


**Fig. 9** Nyquist plot of PANi, $V_2O_5$, and $V_2O_5$-PANi electrodeposited on Nickel foam

the stability of the composite. Moreover, the perpetuation of CV shape at higher sweep rates is a better evidence of the good reversibility of composite material. The CV loop area and current density at each peak increase with increasing scan rates, representing good rate property of the composite electrode [51]. Figure 6b shows the composite material deposited on nickel foam cycled repeatedly for about 200 cycles at a scan rate of 100 mV/s to check their electrochemical stability. No abrupt change in the currents, voltage, and shape of the cyclic voltammograms confirmed the stability of the composite.

To further investigate the capacitance of $V_2O_5$-PANi composite, the galvanostatic charge-discharge (GCD) test was carried out from − 1 to 1.5 V vs. SCE in 0.5 M $LiClO_4$ in propylene carbonate solution. The first GCD curves of pure PANi, $V_2O_5$, and $V_2O_5$-PANi composite carried out at 1 mA/cm$^2$ are shown in Fig. 7a. The GCD curve shows non-linearity suggesting redox process during discharge [52]. The slope of the DC curve possesses two specific portions verifying the pseudocapacitive behavior: the portion of slope parallel to the y-axis designates the IR drop (voltage change) while the remaining portion of the slope is associated with the capacitive component. The GCD curve of $V_2O_5$-PANi composite shows a smaller IR drop than PANi and $V_2O_5$ indicating smaller contact resistance in the former case. To achieve higher energy densities, it is useful to achieve a higher potential window for a supercapacitor electrode. These higher operating potential windows cannot be achieved in the case of aqueous electrolytes. Therefore, organic electrolytes, propylene carbonate-based electrolytes, have been used to serve the purpose. However, high resistance of the later class hindered the mobility of ions. In addition to this, the pore resistance offered by an electrode towards organic electrolyte is higher than that of aqueous one, resulting in larger values of the IR drop, especially at higher current densities. The discharge time of $V_2O_5$-PANi composite is much higher than that of $V_2O_5$ and PANi separately indicating its better electrochemical performance. GCD test of the composite was performed at different current densities as shown in Fig. 7b. $V_2O_5$-PANi exhibited specific capacitance of 1115, 1087, 998, 875, 768, and 689 F/g at a current density of 1, 1.5, 2, 2.5, 3, and 3.5 A/g, respectively (calculated using Eq. 1). The highest specific capacitance reported previously for $V_2O_5$-PANi composite are given in Table 1. A decrease in the specific capacitance has been observed with increasing current densities as shown in Fig. 7d. When charges are injected at high rates and higher currents, the mass of the involved ions probably do not find enough time to utilize the bulk of the material and only the surface layer of composite contribute to charge-discharge processes [53, 54]. Moreover, with increasing current density, an increase in the IR drop has also been observed. The

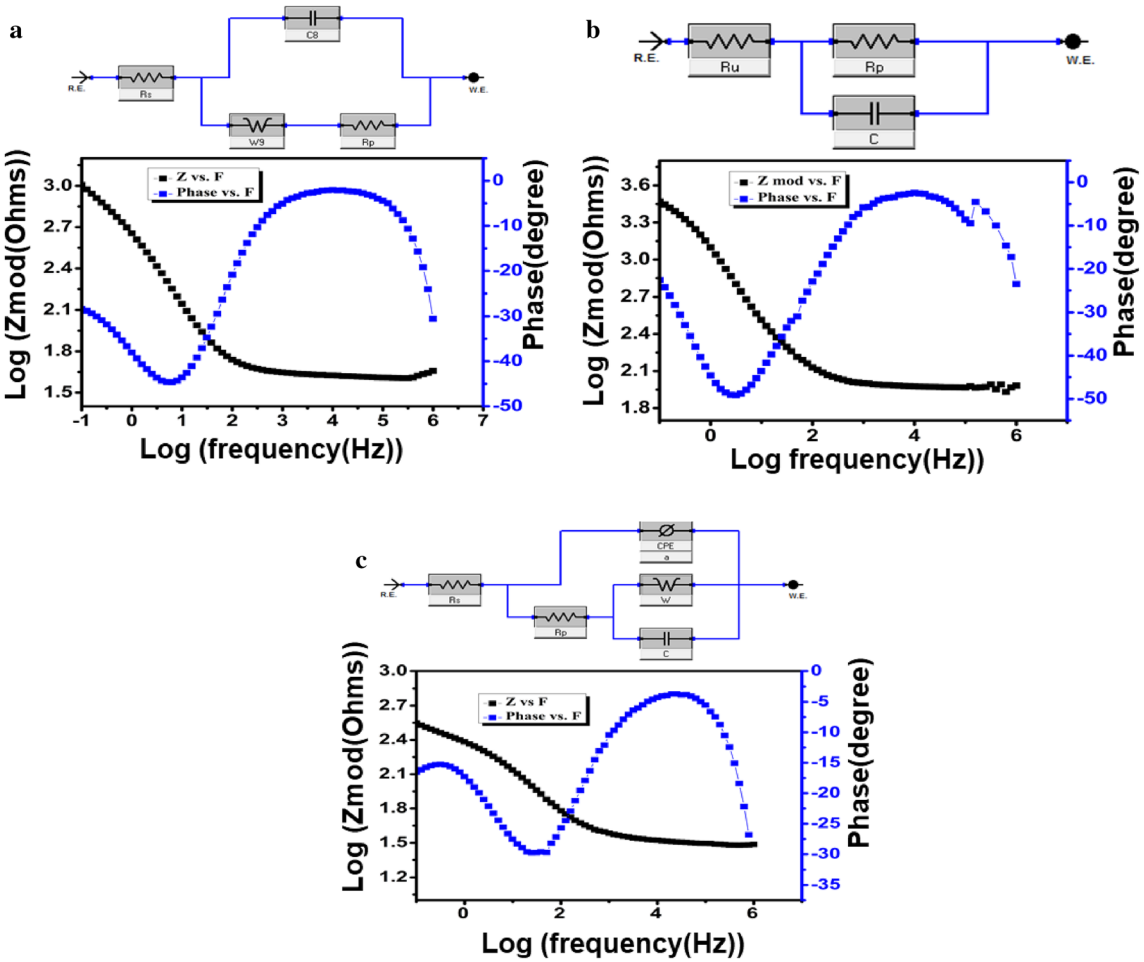


**Fig. 10** Bode plot of EIS spectra of **a** $V_2O_5$, **b** PANi and **c** $V_2O_5$-PANi with corresponding circuit model above each

equivalent series resistance (ESR) value for all the series electrodes were also calculated from GCD plot engaged at 1 A/g according to the following formula [55]:

$$\mathrm{ESR} = \frac{\Delta V}{2I} \tag{2}$$

where $\Delta V$ is the potential drop and $I$ is the current at which the GCD is obtained. The ESR values for PANi, $V_2O_5$ and $V_2O_5$-PANi composite were 0.667, 0.65.and 0.55 ohms, respectively.

The capacitance retention of the composite is displayed as a function of cycle number in Fig. 7c where the material shows a decrease in retention of capacitance after 2000 and 4000 cycles. The material retained a capacitance of up to 90% even after 4000 cycles that can be attributed to the excellent synergistic effect of composite and their good adherence to the Nickel foam substrate. Furthermore, an asymmetric device consisting of 1 $cm^2$ deposited $V_2O_5$-PANi composite electrode and graphite electrode separated by a cellulose paper separator was assembled and soaked in the electrolyte for 30 min before testing. The response of the device is presented in the supplementary video where 3 LED lights were used to demonstrate the charge storage ability of the deposited electrodes (Fig. 8).

Figure 9 shows the Nyquist plot of PANi, $V_2O_5$, and $V_2O_5$_PANi composite deposited on Nickel foam. The corresponding models used to fit the curve using Echem analyst are shown in Fig. 9. Electrochemical impedance spectroscopy (EIS) was carried in a three-electrodes setup, with 0-volt DC vs. open circuit potential and an AC voltage of 10 mV (root mean square). The bode plots of EIS spectra for PANi, $V_2O_5$, and $V_2O_5$_PANi are shown in Fig. 10a–c, respectively with their corresponding circuit model shown as an inset. The bode plot of PANi is fitted with a simple Randle model with a single time

constant i.e. $R_p$(Polarization resistance) in parallel with a double-layer capacitor which is in good accordance with the Nyquist as shown in Fig. 9 (a semi-circle). Bode plot for $V_2O_5$ also has one single time constant with a broad peak at relatively higher frequencies than that of PANi because of higher resistance due to the highly porous structure of $V_2O_5$ than PANi. Figure 10c shows the bode plot of $V_2O_5$_PANi with an equivalent circuit model. This model contains two-time constants, a charge transfer resistance ($R_{ct}$) is paralleled by a capacitor behaving like a CPE (constant phase element) and a Warburg Impedance paralleled by a capacitor. In the oxides layer, if the non-uniform porous structure is intruded by a uniform porous matrix the resulting EIS spectra appear with two-time constants instead of one time constant due to decreased resistance of ions inside porous materials [56]. This behavior of two-time constants can be seen in both the bode plot (two peaks in phase vs. frequency plot) and in the Nyquist plot (two semicircular types Nyquist plot). The appearance of 2nd time constant for $V_2O_5$_PANi shows a decrease in the charge transfer resistance due to the existence of PANi matrix inside a porous $V_2O_5$ structure.

## 4 Conclusions

In summary, a facile electro-codeposition technique has been carried out for the successful deposition of $V_2O_5$-PANi composite through cyclic voltammetry on 3D Nickel foam substrate as a current collector without using any binder. $V_2O_5$-PANi composite displayed a very wide voltage window of 2.5 V for charge storage and highest specific capacitance of 1115 F/g at a current density of 1 A/g. The enhanced electrochemical activity of $V_2O_5$-PANi composite than pure metal oxide and PANi can be attributed to their synergistic effect. The $V_2O_5$-PANi composite can be a better candidate to be used in high-performance pseudocapacitors.

## Acknowledgements

We acknowledge the Higher Education Commission of Pakistan for financial support.

## Compliance with ethical standards

**Conflict of interest** The authors declare that they have no conflict of interest.

## References

1. F. Meng, Y. Ding, Sub-micrometer-thick all-solid-state supercapacitors with high power and energy densities. Adv. Mater. **23**, 4098–4102 (2011)
2. W. Qiong, X. Yuxi, Supercapacitors based on flexible graphene/polyaniline nanofiber composite film. ACS Nano **4**, 1963–1970 (2010)
3. Z. Weng, Y. Su, D.W. Wang, F. Li, J. Du, Graphene–cellulose paper flexible supercapacitors. Adv. Energy Mater. **1**, 917–922 (2011)
4. S. Hussain, X. Yang, M.K. Aslam, A. Shaheen, M.S. Javed, N. Aslam, Robust TiN nanoparticles polysulfide anchor for Li–S storage and diffusion pathways using first principle calculations. Chem. Eng. J. **391**, 123595 (2020)
5. B. Zou, Y. Liang, X. Liu, Electrodeposition and pseudocapacitive properties of tungsten oxide/polyaniline composite. J. Power Sources. **196**, 4842–4848 (2011)
6. C. Peng, S. Zhang, G.Z. Chen, Carbon nanotube and conducting polymer composites for supercapacitors. Prog. Nat. Sci. **18**, 777–788 (2008)
7. S. Sarangapani, B.V. Tilak, C.P. Chen, Materials for electrochemical capacitors theoretical and experimental constraints. J. Electrochem. Soc. **143**, 3791 (1996)
8. J. Hwang, H.M. Kim, S. Shin, Designing a high-performance lithium–sulfur batteries based on layered double hydroxides–carbon nanotubes composite cathode and a dual-functional graphene– polypropylene–$Al_2O_3$ separator. Adv. Funct. Mater. **28**, 1704294 (2018)
9. H. Liu, D. Zhao, Y. Liu, P. Hu, X. Wu, H. Xia, Boosting energy storage and electrocatalytic performances by synergizing CoMoO4@MoZn22 core-shell structures. Chem. Eng. J. **373**, 485–492 (2019)
10. L.L. Zhang, R. Zhou, Graphene-based materials as supercapacitor electrodes. J. Mater Chem. **20**, 5983–5992 (2010)
11. C. Soc, G. Wang, A review of electrode materials for electrochemical supercapacitors. J. Chem Soc Rev. **41**, 797–828 (2012)
12. Y. Zhai, Y. Dou, R.T. Mayes, Carbon materials for chemical capacitive energy storage. Adv. Mater. **23**, 4828–4850 (2011)
13. K. Zhang, L.L. Zhang, J. Wu, Graphene/polyaniline nanofiber composites as supercapacitor electrodes. Chem. Mater. **22**, 1392–1401 (2010)
14. P.C. Huai, C.R. Xiao, W. Ping, Flexible graphene–polyaniline composite paper for High performance supercapacitor. Energy Environ. Sci. **6**, 1185 (2013)

15. S. Hussain, M.S. Javed, S. Asim, A. Shaheen, Y. Abbas, A. Iqbal, M. Wang, Novel gravel-like $NiMoO_4$ nanoparticles on carbon cloth for outstanding supercapacitor applications. Ceram. Int. **46**, 6406–6412 (2020)
16. C. Liu, X. Wu, B. Wang, Performance modulation of energy storage devices: a case of Ni-Co-S electrode materials. Chem. Eng. J. **392**, 123651 (2020)
17. W. Fan, Z. Chao, W. Weng, Graphene-wrapped polyaniline hollow spheres as novel hybrid electrode materials for supercapacitor applications. ACS Appl. Mater. Interfaces. **58**, 3382–3391 (2013)
18. Z. Chengzhou, Z. Junfeng, D. Shaojun, Graphene oxide/polypyrrole nanocomposites: one-step electrochemical doping, coating and synergistic effect for energy storage. J. Mater. Chem. **22**, 6300–6306 (2012)
19. Z. Guoyin, H. Zhi, C. Jun, Highly conductive three-dimensional $MnO_2$– carbon nanotube–graphene–Ni hybrid foam as a binder-free supercapacitor electrode. Nanoscale. **6**, 1079–1085 (2014)
20. Z. Zheye, C. Kai, X. Fei, Advanced solid-state asymmetric supercapacitors based on 3D graphene/$MnO_2$ and graphene/polypyrrole hybrid architectures. J. Mater. Chem. **A**. **3**, 12828–12835 (2015)
21. Z. Zhang, X. Fei, Facile synthesis of 3D $MnO_2$–graphene and carbon nanotube graphene composite networks for high-performance, flexible, all-solid-state asymmetric supercapacitors. Adv. Energy Mater. **1400064**, 1–9 (2014)
22. J. Lee, H.M. Pathan, O. Joo, Electrochemical capacitance of nanocomposite films formed by loading carbon nanotubes with ruthenium oxide. J. Power. Sources. **159**, 1527–1531 (2006)
23. S.G. Kandalkar, J.L. Gunjakar, Preparation of cobalt oxide thin films and its use insupercapacitor application. Appl. Surface Sci. **254**, 5540–5544 (2008)
24. Y. Zheng, H. Ding, M. Zhang, Preparation and electrochemical properties of nickel oxide as a supercapacitor electrode material. Mater. Res. Bull. **44**, 403–407 (2009)
25. G. Lota, E. Frackowiak, M. Monthioux, High performance supercapacitor from chromium oxide-nanotubes based electrodes. Chemical. Phy. Lett. **434**, 73–77 (2007)
26. J. Chang, C. Huang, W.T. Tsai, M.J. Deng, I.W. Sun, Manganese films electrodeposited at different potentials and temperatures in ionic liquid and their application as electrode materials for supercapacitors. Electrochimic. Acta. **53**, 4447–4453 (2008)
27. D. Zhoa, M. Dai, H. Liu, D. Xue, X. Wu, J. Liu, Sulfur-induced interface engineering of hybrid $NiCo_2O_4$@ $NiMo_2S_4$ structure for overall water splitting and flexible hybrid energy storage. Adv. Mater. Interfaces. 1901308 (2019).
28. Y. Zhoa, J. He, M. Dai, D. Zhoa, X. Wu, B. Liu, Emerging CoMn-LDH@MnO2 electrode materials assembled using nanosheets for flexible and foldable energy storage devices. J. Energy. Chem. **45**, 67–73 (2020)
29. D. Zhoa, H. Liu, X. Wu, Bi-interface induced multi-active $MCo_2O_4$@$MCo_2S_4$@PPy (M=Ni, Zn) sandwich structure for energy storage and electrocatalysis. Nano Energy. **57**, 363 (2019)
30. W.F. Mak, G. Wee, V. Aravindan, High-energy density asymmetric supercapacitor based on electrospun vanadium pentoxide and polyaniline nanofibers in aqueous electrolyte. J. Electrochem. Soc. **159**, 1481–1488 (2012)
31. Q. Qu, Y. Zhu, X. Gao, Core – Shell structure of polypyrrole grown on $V_2O_5$ nanoribbon as high performance anode material for supercapacitors. Adv. Energy. Mater. **2**, 950–955 (2012)
32. V. Gupta, N. Miura, High performance electrochemical supercapacitor from electrochemically synthesized nanostructured polyaniline. Mater. Lett. **60**, 1466–1469 (2006)
33. B.M. Hughes, C. Annette, Electrochemical capacitance of nanocomposite films formed by coating aligned arrays of carbon nanotubes with polypyrrole. Adv Matt. **14**, 382–385 (2002)
34. G. Wang, A. Vanchiappan, G. Nutan, LiCl/PVA gel electrolyte stabilizes vanadium oxide nanowire electrodes for pseudocapacitors. J. Electrochem. Soc. **159**, 1481–1488 (2012)
35. S.Y. Lee, J. Kim, S. Park, Activated carbon nanotubes/polyaniline composites as supercapacitor electrodes. Energy. **78**, 298–303 (2014)
36. W.-C. Chen, T.-C. Wen, H. Teng, Polyaniline-deposited porous carbon electrode for Supercapacitor. Electrochimic. Acta. **48**, 641–649 (2003)
37. A. Janke, M. Stamm, M. Bo, Vertically oriented arrays of polyaniline nanorods and their super electrochemical properties. Chem. Commun. **38**, 5749–5751 (2009)
38. A. Gonzalez, E. Goikolea, J. Andoni, Review on supercapacitors: technologies and materials. Renew. Sust. Energ. Rev. **58**, 1189–1206 (2016)
39. Y. Huo, H. Zhang, J. Jiang, A three-dimensional nanostructured PANI/MnOx porous microsphere and its capacitive performance. J. Mater. Sci. **47**, 7026–7034 (2012)
40. B. Ming, L. Tian, L. Feng, Electro-codeposition of vanadium oxide-polyaniline composite nanowire electrodes for high energy density supercapacitors. J. Mater. Chem. A. **2**, 10882–10888 (2014)
41. S. Hussain, M.S. Javed, A. Shaheen, N. Aslam, Y. Abbas, I. Ashraf, M. Wang, Unique hierarchical mesoporous $LaCrO_3$ perovskite oxides for highly efficient electrochemical energy storage applications. Ceram. Int. **45**, 15164 (2019)

42. A. Mostafaei, A. Zolriasatein, Synthesis and characterization of conducting polyaniline nanocomposites containing ZnO nanorods. Prog. Nat. Sci. Mater. Int. **22**, 273–280 (2012)
43. S.B. Kondawar, S.P. Agrawal, Transport properties of conductive polyaniline nanocomposites based on carbon nanotubes. Inter. J. Compos. Mater. **2**, 32–36 (2012)
44. L. Ding, Q. Li, D. Zhou, H. Cui, H. An, Modification of glassy carbon electrode with polyaniline/multi-walled carbon nanotubes composite: application to electro-reduction of bromate. J. Electroanal. Chem. **668**, 44–50 (2012)
45. S.H. Patil, A.P. Gaikwad, S.D. Sathaye, To form layer by layer composite film in view of its application as supercapacitor electrode by exploiting the techniques of thin films formation just around the corner. Electrochimic. Acta. **265**, 556–568 (2018)
46. K. Liang, X. Tang, W. Hu, Y. Yang, Ultrafine V2O5 nanowires in 3D current collector for high performance supercapacitor. ChemElectroChem. **3**, 704–708 (2016)
47. V. Maurice, S. Zanna, L. Klein, XPS study of Li ion intercalation in $V_2O_5$ thin films prepared by thermal oxidation of vanadium metal. Electrochimic. Acta. **52**, 5644–5653 (2007)
48. Y. Wang, G. Cao, Li + -intercalation electrochemical/electrochromic properties of vanadium pentoxide films by sol electrophoretic deposition. Electrochimic. Acta. **51**, 4865–4872 (2006)
49. X. Liu, L. Bian, L. Zhang, Composite films of polyaniline and molybdenum oxide formed by electrocodeposition in aqueous media. J. solid state electrochem. **11**, 1279–1286 (2007)
50. V.J. Vijakumar, M.K. Rohan, D.T. Nanasaheb, J.M. Yun, K.H. Kim, R.S. Mane, Annealing environment effects on the electrochemical behavior of supercapacitors using Ni foam current collectors. Mater. Res. Express. **5**, 125004 (2018)
51. J. Kim, Synthesis and enhanced electrochemical supercapacitor properties of Ag-$MnO_2$-polyaniline nanocomposite electrodes. Energy. **70**, 473–477 (2014)
52. Y. Zhang, Synthesis of novel graphene oxide/pristine graphene/polyaniline ternary composites and application to supercapacitor. Chem. Eng. J. **288**, 689–700 (2016)
53. W. Gongming, L. Xihong, Z. Teng, LiCl/PVA gel electrolyte stabilizes vanadium oxide nanowire electrodes for pseudocapacitors. ACS Nano **6**, 10296–10302 (2012)
54. F. Gobal, M. Faraji, Electrodeposited polyaniline on Pd-loaded $TiO_2$ nanotubes as active material for electrochemical supercapacitor. J. Electroanal. Chem. **691**, 51–56 (2013)
55. R. Vacentini, L.M.D. Silva, E.P. Junior, W.G. Nunes, How to measure and calculate equivalent series resistance of electric double-layer capacitors. Molecules **24**, 1452 (2019)
56. B. Diaz, L. Freire, M. Mujio, X.R. Novoa, Optimization of conversion coatings based on zinc phosphate on high strength steels, with enhanced barrier properties. J. Electroanal Chem. **737**, 174–183 (2015)
57. A. Roy, A. Ray, P. Sadhukhan, S. Saha, S. Das, Morphological behaviour, electronic bond formation and electrochemical performance study of $V_2O_5$-polyaniline composite and its application in asymmetric supercapacitor. Mater. Res. Bull. **107**, 379–390 (2018)